The Astronomical Journal, 148:77 (12pp), 2014 November doi:10.1088/0004-6256/148/5/77

COLOR–MASS-TO-LIGHT-RATIO RELATIONS FOR DISK GALAXIES

Stacy S. McGaugh[1] and James M. Schombert[2]
[1] Department of Astronomy, Case Western Reserve University, Cleveland, OH 44106, USA; stacy.mcgaugh@case.edu
[2] Department of Physics, University of Oregon, Eugene, OR 97403, USA; jschombe@uoregon.edu
Received 2013 March 1; accepted 2014 July 7; published 2014 September 19

ABSTRACT

We combine *Spitzer* 3.6 μm observations of a sample of disk galaxies spanning over 10 mag in luminosity with optical luminosities and colors to test population synthesis prescriptions for computing stellar mass. Many commonly employed models fail to provide self-consistent results: the stellar mass estimated from the luminosity in one band can differ grossly from that of another band for the same galaxy. Independent models agree closely in the optical (V band), but diverge at longer wavelengths. This effect is particularly pronounced in recent models with substantial contributions from TP-AGB stars. We provide revised color–mass-to-light ratio relations that yield self-consistent stellar masses when applied to real galaxies. The $B-V$ color is a good indicator of the mass-to-light ratio. Some additional information is provided by $V-I$, but neither it nor $J-K_s$ are particularly useful for constraining the mass-to-light ratio on their own. In the near-infrared, the mass-to-light ratio depends weakly on color, with typical values of 0.6 $M_\odot/L_\odot$ in the K_s band and 0.47 $M_\odot/L_\odot$ at 3.6 μm.

Key words: galaxies: evolution – galaxies: fundamental parameters – galaxies: photometry – galaxies: stellar content

Online-only material: color figures

1. INTRODUCTION

One of the most fundamental properties of a galaxy is its luminosity and the mass of the stars that produce it. Our understanding of stellar evolution is sufficiently advanced that it should be possible to compute the luminosity produced by a stellar population ab initio (e.g, Bruzual & Charlot 2003; Le Borgne et al. 2004). Indeed, there exist in the literature various prescriptions for estimating stellar mass from observed colors or spectral energy distributions (SEDs; e.g., Bell & de Jong 2001; Bell et al. 2003; Portinari et al. 2004; Zibetti et al. 2009; Into & Portinari 2013).

A general expectation of population synthesis models is that the relation between mass and light is more nearly constant in the near-infrared (NIR) than in the optical part of the spectrum. This follows from basic considerations: recent star formation populates the upper main sequence with luminous, blue stars. These stars produce copious amounts of optical light from little mass and lead short lives, causing substantial perturbations to the average mass-to-light ratio Υ_* of a galaxy. The degree to which this occurs depends on the IMF and the intensity of a star forming event relative to the total stellar mass already present. These effects combine to make the prediction of any particular galaxy's optical mass-to-light ratio uncertain by a factor of a few. Young stars contribute rather less in the NIR part of the spectrum, so one expects a closer relation between light and mass at these wavelengths. Empirically, the scatter in the Tully–Fisher relation declines as one goes from blue to red to NIR wavelengths (Verheijen 2001), consistent with the expected decrease in scatter in Υ_*.

In this paper we use 3.6 μm *Spitzer Space Telescope* photometry (Schombert & McGaugh 2014b) of a sample of galaxies spanning a large range (ten magnitudes) in luminosity. We combine these data with optical colors and luminosities to check the predictions of several population synthesis models. Extant models return systematically different stellar masses when applied to the optical and NIR luminosity of the same galaxy.

We describe the data in Section 2. In Section 3 we discuss various population synthesis models and apply them to the data to compute stellar masses in Section 4. In Section 5 we determine what is required for each model to produce self-consistent results, and present revised color–mass-to-light-ratio relations (CMLR) the provide an improved prescription for estimating stellar mass from photometric data. We discuss our results and compare them to other constraints in Section 6 and summarize in Section 7.

2. DATA

The SINGS (Kennicutt et al. 2003; Dale et al. 2005) and THINGS (Walter et al. 2008; de Blok et al. 2008) surveys have demonstrated the utility of *Spitzer* 3.6 μm data for constraining the stellar components of star forming galaxies. Here we wish to sample disk galaxies over as large a range of physical properties as possible. To this end, we combine the THINGS data of de Blok et al. (2008) with new data from two *Spitzer* programs. One cycle 5 project targeted galaxies to increase the sampling of both higher and lower masses than present in THINGS. A cycle 7 snapshot program provides additional photometry for low surface brightness galaxies (Schombert & McGaugh 2014b). The combined sample spans 10 mag in [3.6] luminosity.

The [3.6] luminosities of galaxies in the THINGS sample have been adopted from the mass models of de Blok et al. (2008). Only the total luminosity is used here. No distinction is made between bulge and disk components.

The remainder of the assembled sample is composed of new *Spitzer* observations obtained by ourselves (Schombert & McGaugh 2014b). The *Spitzer* data have been analyzed with the ARCHANGEL surface photometry package (Schombert 2011). Elliptical isophotes have been fit to the data and integrated magnitudes determined from asymptotic fits to curves of growth. Special care has been taken to exclude foreground stars and background galaxies and replace the masked region with an estimate of the galaxy light based on surrounding pixels.

IRAC is a sensitive instrument, and many background galaxies shine through the disks of the target galaxies at 3.6 μm. Careful cleaning of these contaminants is essential to accurate photometry. Once this step is taken, total magnitudes can be determined to a few hundredths of a magnitude. Colors and magnitudes are corrected for Galactic extinction using the calibration of Schlafly & Finkbeiner (2011). Internal extinction corrections follow the RC3 convention (de Vaucouleurs et al. 1991), but this is only substantial (≈0.2 mag) in the brightest few galaxies.

We assume that the observed NIR light is stellar in origin and make no attempt to correct for nonstellar contamination (e.g., PAH emission). This is small at 3.6 μm (Kim et al. 2012; Meidt et al. 2012). Indeed, for the galaxies detected by IRAS, the observations of Kim et al. (2012) can be used to estimate the amount of contamination expected from the 3.3 μm PAH feature. In all cases, it is expected to be <2% of the observed flux, and usually much less than 1% (J. H. Kim 2013, private communication). It will be less for the low surface brightness galaxies not detected by IRAS.

The data are presented in Table 1. For each galaxy, we assign a distance and compute the corresponding absolute magnitude in the optical V band and NIR *Spitzer* IRAC [3.6] band. Distances are taken from the direct measurements tabulated in the Extragalactic Distance Database (Tully et al. 2009) when available. When no direct distance measurement is known, a Hubble flow distance assuming $H_0 = 75$ km s^{-1} Mpc^{-1} is adopted. Measured colors are given where known. The majority of the sample have observed $B-V$ colors. For brighter galaxies, $J-K_s$ can readily be extracted from 2MASS (Jarrett et al. 2000). The lower surface brightness galaxies are typically not detected[3] by 2MASS. For many, $V-I$ has been observed (Schombert et al. 2011). The colors quoted there were based on fixed apertures; here, we adopted a weighted average to better represent the extended low surface brightness portions of the disks. The isophotal weighted and aperture colors rarely differed by more than 0.05 mag except where a prominent bulge component was present. References to the sources of these data are given in the final column of Table 1.

Table 1
Galaxy Data

Galaxy	D	M_V	$M_{[3.6]}$	$B-V$	$V-I$	$J-K_s$	Refs.
DDO 154	4.04	−14.45	−16.41	0.32	0.14	0.34	1, 2, 3, 4, 5, 6
D631-7	5.49	−14.50	−16.73	0.41	0.55	...	1, 7
D568-2	21.3	−14.6	−16.81	0.45	0.70	...	1, 3
D572-5	14.6	−14.56	−16.82	0.44	0.52	...	1, 7
F415-3	10.4	−15.2	−16.99	0.62	0.71	...	1, 8
DDO 168	4.25	−15.70	−17.45	0.32	...	...	1, 3, 9
F611-1	25.5	−15.4	−17.92	0.57	...	...	1, 8
D500-2	17.9	−16.38	−18.25	0.52	0.42	...	1, 7
F565-V2	55.1	−16.2	−18.76	0.44	...	...	1, 8
NGC 2366	3.27	−16.82	−18.90	0.54	0.52	0.84	2, 5, 6, 9
D723-5	27.7	−16.9	−19.21	0.55	0.75	...	1, 3
F563-V1	57.6	−17.2	−19.79	0.23	0.83	...	1, 8
IC 2574	3.91	−17.70	−20.15	0.42	0.67	0.58	2, 5, 6, 8
F563-1	52.2	−17.8	−20.40	0.40	0.86	...	1, 8
F574-2	92.3	−18.3	−20.50	0.58	...	...	1, 8
NGC 2976	3.58	−17.80	−20.52	0.55	0.67	0.79	2, 5, 6, 10
F568-V1	84.8	−18.6	−20.82	0.47	0.70	...	1, 8, 11
F561-1	69.8	−18.3	−20.88	0.69	0.72	...	1, 3, 8
F577-V1	113.	−18.7	−20.95	0.50	1.07	...	1, 3, 8
NGC 1003	10.2	−18.79	−21.12	0.42	...	0.73	2, 5, 6
UGC 5005	57.1	−18.7	−21.18	0.35	...	...	1, 8
F574-1	100.	−19.1	−21.37	0.51	...	...	1, 8
F568-1	95.5	−18.9	−21.38	0.52	0.70	...	1, 8, 11
NGC 7793	3.61	−18.86	−21.46	0.63	0.20	0.68	2, 5, 6
UGC 128	58.5	−19.3	−21.88	0.63	0.68	...	1, 11
NGC 2403	3.16	−19.14	−21.97	0.39	1.03	0.75	2, 5, 6, 10
NGC 925	9.43	−19.97	−22.30	0.50	0.75	0.83	2, 5, 6, 10
NGC 2903	8.9	−20.82	−22.74	0.55	1.16	0.91	2, 5, 6, 12
NGC 3198	13.8	−20.40	−23.00	0.43	1.02	0.92	2, 5, 6, 12
NGC 3621	6.56	−19.74	−23.04	0.52	0.81	0.83	2, 5, 6
NGC 3521	8.0	−20.65	−24.19	0.68	1.18	0.93	2, 5, 6, 10
NGC 3031	3.65	−21.08	−24.28	0.82	1.31	0.88	2, 5, 6, 10
NGC 5055	8.99	−21.22	−24.60	0.64	1.21	0.95	2, 5, 6, 10
NGC 2998	68.3	−22.36	−24.77	0.45	...	0.99	2, 5, 6
NGC 2841	14.1	−21.57	−24.88	0.74	1.35	0.93	2, 5, 6, 10
NGC 6674	51.9	−22.17	−25.17	0.57	...	0.86	2, 5, 6
NGC 7331	14.9	−21.63	−25.30	0.63	1.36	1.00	2, 5, 6, 10
NGC 801	75.3	−22.30	−25.33	0.61	...	1.05	2, 5, 6, 9
NGC 5533	59.4	−22.16	−25.47	0.77	...	0.94	2, 5, 6
UGC 2885	75.9	−23.30	−25.94	0.47	...	0.88	1, 5, 6

Notes. Galaxy photometric data in order of increasing [3.6] luminosity. Adopted distances are in Mpc. $H_0 = 75$ km s^{-1} Mpc^{-1} is assumed when no direct determination is available. We adopt $M_\odot^V = 4.83$, $M_\odot^I = 4.08$, and $M_\odot^{[3.6]} = 3.24$.

References. *Spitzer* [3.6] mag: (1) Schombert & McGaugh (2014b), (2) de Blok et al. (2008). Ancillary data: (3) Schombert et al. (2011), (4) Dale et al. (2007), (5) de Vaucouleurs et al. (1991), (6) Jarrett et al. (2000), (7) Trachternach et al. (2009), (8) McGaugh & Bothun (1994), (9) Makarova (1999), (10) Muñoz-Mateos et al. (2009), (11) de Blok et al. (1995), (12) Fisher & Drory (2008).

3. POPULATION SYNTHESIS MODELS

Our knowledge of stellar evolution is sufficiently advanced to enable the ab initio calculation of the spectral energy distribution (SED) of stellar populations. Considerable effort has gone into the development of stellar population synthesis models that do just this (e.g., Bruzual & Charlot 2003). Outstanding progress has been made, and it has become standard practice to quote stellar masses for galaxies based on fits to multi-color data with such models.

The accuracy with which stellar masses can be estimated is debatable, but is probably no better than a factor of two. Outstanding problems include uncertainty in the IMF, variations in the star formation histories of galaxies, the distribution of stellar metallicities, and the contribution of stars in bright but short-lived phases of evolution (e.g., TP-AGB stars). Here we compare the predictions of various models with each other. We also check their internal self-consistency to gauge the extent to which the same model predicts the same stellar mass for the same galaxy when the luminosity is measured in different bands.

A simple approach to estimating the stellar mass of a galaxy is to assume a single, constant mass-to-light ratio Υ_* such that $M_* = \Upsilon_* L$. This is a crude approximation, as we expect the mass-to-light ratio of a population to vary with age and, to a lesser extent, with metallicity. For example, using a mutli-metallicity model (Schombert & Rakos 2009; Schombert & McGaugh 2014a), we find that a 12 Gyr old stellar population of solar metallicity has $\Upsilon_*^V = 2.8\ M_\odot/L_\odot$, while a stellar population with the same age but peak [Fe/H] = −1.5 has $\Upsilon_*^V = 1.8\ M_\odot/L_\odot$. That same solar metallicity stellar population has Υ_*^V of only 0.4 $M_\odot/L_\odot$ at an age of 1 Gyr.

[3] DDO 154 is only marginally detected by 2MASS, so we are skeptical of its $J-K_s$ color. Colors measured by ourselves are good to a few hundredths of a magnitude and intercomparison of other modern photometry (e.g., Dale et al. 2007; Muñoz-Mateos et al. 2009) is similarly encouraging.

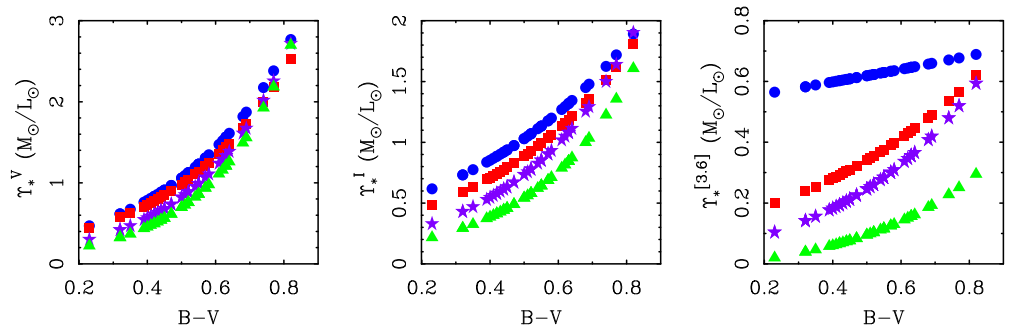

Figure 1. Relation between $B-V$ color and the stellar mass-to-light ratio in the V band (left), I band (center), and the *Spitzer* [3.6] band (right) from the population synthesis models of Bell et al. (2003) with their scaled Salpeter IMF (circles), Portinari et al. (2004) with a Kroupa (1998) IMF (squares), Zibetti et al. (2009) with a Chabrier (2003) IMF (triangles), and Into & Portinari (2013) with a Kroupa (1998) IMF (stars). The formula of Oh et al. (2008, Equation (2)) is used to convert between K_s and [3.6]. Note the large disparity between models in the NIR.

(A color version of this figure is available in the online journal.)

Table 2
Population Synthesis CMLR

Model	IMF	a_V	b_V	a_I	b_I	a_K	b_K	$\Upsilon^V_{0.6}$	$\Upsilon^I_{0.6}$	$\Upsilon^K_{0.6}$	$\Upsilon^{[3.6]}_{0.6}$	AGB
Bell et al. (2003)	Scaled Salpeter	−0.628	1.305	−0.399	0.824	−0.206	0.135	1.43	1.25	0.73	0.62	old
Portinari et al. (2004)	Kroupa (1998)	−0.654	1.290	−0.537	0.970	−0.736	0.730	1.32	1.11	0.50	0.41	old
Zibetti et al. (2009)	Chabrier (2003)	−1.075	1.837	−1.003	1.475	−1.390	1.176	1.07	0.76	0.21	0.14	new
Into & Portinari (2013)	Kroupa (1998)	−0.900	1.627	−0.782	1.294	−1.020	1.054	1.19	0.99	0.41	0.33	new

Notes. Stellar mass-to-light ratios in the V, I, and K bands as given by various population synthesis models in solar units through the formula $\log \Upsilon^i_* = a_i + b_i(B-V)$. For reference, the mass-to-light ratios predicted by each model for $B-V=0.6$ are also given. The AGB column denotes whether the model includes older or newer (Marigo et al. 2008) prescriptions for TP-AGB stars.

A more sophisticated approach is to use a population synthesis model to construct a CMLR. This relates the mean mass-to-light ratio Υ^i_* in band i to a color $(m_j - m_k)$ through

$$\log \Upsilon^i_* = a_i + b_i(m_j - m_k). \quad (1)$$

The bands i, j, k can be independent, but need not be. That is, sometimes band $i = j$ or k.

Using a color as a mass-to-light ratio estimator reduces to the simple approach if the slope b is small for some band i. Variation of Υ_* with color is expected to be minimized in the NIR. Similarly, we expect optical colors to provide an indicator of Υ_*. For the multi-metallicity models of Schombert & Rakos (2009), we find that the solar metallicity model changes in color as it ages from 1 to 12 Gyr by $\Delta(B-V)=0.37$ and $\Delta(J-K)=0.03$. Thus we expect $B-V$ to be a more sensitive indicator of Υ_* than $J-K_s$.

There should be some intrinsic scatter about the mean CMLR. This scatter ultimately limits the accuracy achievable by this approach, but is expected to be minimized in the NIR (Bell & de Jong 2001). One might hope to do better by using multi-color information (e.g., Zibetti et al. 2009), or fitting the entire SED. The accuracy of stellar masses inferred from SED fitting is, however, limited by the fidelity of the population synthesis model to which the SED is fit. This approach will suffer systematic error if a model differs from reality as a function of wavelength.

The coefficients a_i and b_i are given in Table 2 for several representative models for the $i = V, I$, and K bands with $B-V$ color. These particular choices are made because the most data are available in these bands. As we shall see, $B-V$ has some value as a predictor of Υ_*, while $V-I$ and $J-K_s$ do not.

The models typically stop at K while we now have a good deal of *Spitzer* [3.6] photometry. We relate the population synthesis predicted K_s-band mass-to-light ratio Υ^K_* to $\Upsilon^{[3.6]}_*$ using the relation of Oh et al. (2008):

$$\Upsilon^{[3.6]}_* = 0.92\Upsilon^K_* - 0.05. \quad (2)$$

This relation is obtained from population synthesis models, in the same spirit as the CMLR in Table 2.

To convert between Υ^K_* to $\Upsilon^{[3.6]}_*$ in the data, we assume $\Upsilon^K_* = 1.29\Upsilon^{[3.6]}_*$. This follows from the mean color $K_s - [3.6] = 0.31 \pm 0.11$ that we obtain for the 74 galaxies of Dale et al. (2005). In the larger S4G sample, we find a weak anticorrelation between $K_s - [3.6]$ and $B-V$ (Schombert & McGaugh 2014a) such that the conversion factor would vary between 1.39 for $B-V=0.3$ and 1.18 for $B-V=0.8$. This range of variation is within the scatter of $K_s - [3.6]$ at a given $B-V$, so we only employ the mean value and do not attempt to estimate $K_s - [3.6]$ from this weak correlation with $B-V$.

Note that the conversion for the data is not identical to that for the models. As we will see, the models do not perform well in reproducing the data in the NIR. We therefore choose to keep the two separate, making the model conversion with a model result and the data conversion with the mean of the data.

Figure 1 shows the mass-to-light ratios for the models given in Table 2. Rather than simply show a line for each model, we plot the galaxy data to emphasize the beads-on-a-string nature of this approach to estimating stellar mass: a single color may provide a reasonable estimate of the mean mass-to-light ratio, but it cannot reproduce the intrinsic scatter that one expects from variations in star formation histories. The scatter is expected to be from 0.1 dex (Bell & de Jong 2001) to 0.15 dex (Portinari et al. 2004) in the K band, and larger in the optical bands. This is an over-simplification, as the scatter may be a function of color, with larger scatter likely in very blue, actively star forming systems. Additionally, the mean CMLR can bend (the

slope becomes much steeper for $B-V<0.55$ in the models of Portinari et al. 2004) or even bifurcate: the line of Bell et al. (2003) splits the difference between distinct branches of high and low Υ_*^K at blue colors in their Figure 20.

Models will differ if they adopt different evolutionary tracks or a different IMF. Both matter for the models considered here. As pointed out by Bell & de Jong (2001), changes in the IMF to include more or fewer low mass stars serve mostly to change the mass without much altering the luminosity or color, so to a decent approximation can be treated as multiplicative shifts in Υ_*. For specificity, we adopt the scaled Salpeter IMF of Bell & de Jong (2001) for the model of Bell et al. (2003). We adopt the Kroupa IMF (Kroupa 1998) for the model of Portinari et al. (2004) and Into & Portinari (2013), while Zibetti et al. (2009) uses the Chabrier IMF (Chabrier 2003).

The models all give a similar run of Υ_* with color in the optical (left panel of Figure 1), with small offsets[4] for the different IMFs as well as other detailed differences. The agreement degrades as we move to redder wavelengths (middle and right panels of Figure 1). There is a huge disparity in the NIR. The model of Bell et al. (2003) has a relatively flat slope with a high normalization $\Upsilon_*^{[3.6]}>0.55\ M_\odot/L_\odot$, while that of Zibetti et al. (2009) has a steep dependence on color (even in the NIR) and a low normalization $\Upsilon_*^{[3.6]}<0.3\ M_\odot/L_\odot$ for the reddest galaxies and $<0.1\ M_\odot/L_\odot$ for many blue galaxies. The model of Into & Portinari (2013) is intermediate between that of Zibetti et al. (2009) and Portinari et al. (2004).

The chief difference in evolutionary tracks between the various models considered here is the inclusion of a large contribution from TP-AGB stars by Zibetti et al. (2009) and Into & Portinari (2013) as advocated by Maraston (2005). These stars are in the latest stages of evolution, being short-lived and rare, but quite bright. Their contribution to the integrated luminosity of stellar populations is most pronounced in the NIR, where they greatly enhance the predicted luminosity of galaxies while doing little to alter the predictions of previous generations of models in the optical portion of the spectrum. This results in the low mass-to-light ratios of the models[5] of Zibetti et al. (2009) and Into & Portinari (2013) in the right-hand panel of Figure 1. These models will obviously give rather different estimates of the stellar mass, especially when applied in the NIR.

4. GALAXY STELLAR MASSES

We use the models in Table 2 with the data in Table 1 to compute the stellar masses of sample galaxies. These are reported in Table 3. For each galaxy, we use the observed $B-V$ color to predict the mass-to-light ratio separately in V, I, and [3.6] for each model. We then use the corresponding luminosity to obtain a stellar mass estimate. This results in 12 distinct mass estimates for each galaxy: three for each of the four models. A similar exercise could be performed using other colors, but we find $V-I$ and $J-K$ to be less satisfactory[6] than $B-V$ as primary Υ_* estimators. We will consider their use as a second color term later.

We can now compare stellar mass estimate from different population synthesis models. The external consistency of the models is fairly good in the optical: examination of Table 3 shows that M_*^V is usually similar across the board. There are small offsets owing largely to differences in the adopted IMF, which mostly affect the normalization a_V. There are also small differences stemming from differences in the slope b_V. More recent models predict a somewhat steeper slope with color. These small differences are to be expected. All in all, the external consistency between models in the V band is encouraging.

We can also check each model for internal self-consistency from band to band. If all is well, the stellar mass estimated for the same galaxy will be the same irrespective of whether the luminosity is measured in the optical or NIR. Intrinsic scatter in the CMLR precludes this from ever being exactly true, but the sample is large enough that we can check whether it is true on average. This is done in Figure 2, which shows the stellar mass estimated from the I band and [3.6] luminosity plotted against that estimated from the V-band luminosity.

The approximate consistency between models in V does not hold in the NIR. Indeed, most of the models are not internally self-consistent: for a given stellar mass, most models overpredict the infrared luminosity relative to the optical luminosity. In other words, the predicted infrared mass-to-light ratios are too small relative to those in the optical.

The data cover many decades in luminosity. Consequently, even a small offset from the line of equality in the logarithmic Figure 2 corresponds to a serious misestimation of the mass-to-light ratio. The semi-empirical model of Bell et al. (2003) is most nearly self-consistent. Indeed, it provides a very good match between V and I bands, with only a small tendency to overpredict the stellar mass from the NIR. The other models all underpredict the stellar mass from the NIR luminosity relative to that in the V band. This problem is particularly severe in the model of Zibetti et al. (2009), which also suffers the same problem in the I band. The offset and change in slope seen in Figure 2 is an indication that both the intercept a_i and slope b_i are misestimated.

The chief difference between older and more recent models is the prescription for TP-AGB stars (Marigo et al. 2008). This prescription appears to grossly overstate the contribution of TP-AGB stars to the NIR luminosity of real galaxies. Apparently the contribution of these luminous but short-lived stars to the integrated energy budget has been overestimated.

Our conclusion concerning the ratio of NIR to optical luminosity is consistent with the findings of other workers. Melbourne et al. (2012) reach a similar conclusion from resolved color–magnitude diagrams of nearby galaxies where individual TP-AGB stars can be identified. Fewer are observed than expected. Kriek et al. (2010) fit Bruzual & Charlot (2003) and Maraston (2005) models to the SEDs of post-starburst galaxies. Both provide a good fit of the optical part of the spectrum ($\lambda<6000$ Å). The Bruzual & Charlot (2003) also fit the data at longer wavelengths, while the model of Maraston (2005) overpredicts the luminosity in this part of the spectrum (see their Figure 3). Similarly, Zibetti et al. (2013) sought to observe the strong spectral features expected from TP-AGB stars in NIR spectra, but did not find them. Modeling of the latest phases of stellar evolution does not yet appear to be sufficiently accurate to confidently predict the NIR spectra of complex stellar populations.

[4] The models of Bell & de Jong (2001) with a scaled Salpeter IMF are barely distinguishable from those of Portinari et al. (2004) with a Kroupa IMF, so we consider only the latter.

[5] Zibetti et al. (2009) advocate using multiband colors to estimate mass-to-light ratios, and their single-color coefficients that are reproduced in Table 2 are only approximations made to facilitate the sort of comparison made here.

[6] Attempts to build the equivalent of Table 3 with these colors not only limit the data set since there are fewer measurements, but also produce noisy and sometimes unphysical results.

Table 3
Stellar Masses from Population Synthesis Models

Galaxy	B03			P04			Z09			IP13		
	M_*^V	M_*^I	$M_*^{[3.6]}$	M_*^V	M_*^I	$M_*^{[3.6]}$	M_*^V	M_*^I	$M_*^{[3.6]}$	M_*^V	M_*^I	$M_*^{[3.6]}$
DDO 154	7.50	7.33	7.63	7.47	7.24	7.24	7.22	6.94	6.45	7.33	7.10	7.01
D631-7	7.64	7.59	7.77	7.67	7.51	7.45	7.41	7.25	6.79	7.50	7.40	7.26
D568-2	7.73	7.73	7.80	7.70	7.65	7.51	7.52	7.41	6.91	7.60	7.55	7.35
D572-5	7.70	7.63	7.81	7.67	7.55	7.51	7.49	7.31	6.89	7.57	7.45	7.34
F415-3	8.19	8.11	7.90	8.16	8.06	7.72	8.08	7.91	7.27	8.12	8.02	7.63
DDO 168	8.00	...	8.04	7.97	...	7.65	7.72	...	6.87	7.83	...	7.43
F611-1	8.21	...	8.27	8.17	...	8.06	8.06	...	7.56	8.12	...	7.94
D500-2	8.53	8.38	8.39	8.50	8.32	8.15	8.36	8.12	7.61	8.43	8.24	8.01
F565-V2	8.36	...	8.58	8.36	...	8.28	8.15	...	7.67	8.23	...	8.11
NGC 2366	8.74	8.61	8.65	8.70	8.55	8.42	8.58	8.36	7.90	8.64	8.48	8.30
D723-5	8.78	8.75	8.78	8.75	8.69	8.56	8.63	8.50	8.05	8.69	8.62	8.43
F563-V1	8.48	8.63	8.96	8.45	8.53	8.51	8.16	8.18	7.51	8.29	8.36	8.23
IC 2574	8.93	8.93	9.14	8.90	8.85	8.82	8.71	8.60	8.18	8.80	8.74	8.64
F563-1	8.95	9.03	9.23	8.91	8.95	8.90	8.71	8.68	8.24	8.80	8.83	8.72
F574-2	9.38	...	9.30	9.35	...	9.10	9.24	...	8.61	9.30	...	8.99
NGC 2976	9.14	9.07	9.30	9.11	9.02	9.08	8.99	8.83	8.57	9.05	8.95	8.96
F568-V1	9.36	9.34	9.41	9.32	9.27	9.13	9.16	9.04	8.55	9.24	9.18	8.98
F561-1	9.52	9.41	9.47	9.49	9.37	9.34	9.44	9.25	8.93	9.47	9.35	9.27
F577-V1	9.44	9.55	9.47	9.40	9.49	9.21	9.26	9.27	8.65	9.33	9.41	9.07
NGC 1003	9.37	...	9.52	9.34	...	9.21	9.14	...	8.57	9.23	...	9.03
UGC 5005	9.24	...	9.54	9.21	...	9.17	8.98	...	8.44	9.08	...	8.96
F574-1	9.61	...	9.64	9.58	...	9.39	9.43	...	8.84	9.50	...	9.25
F568-1	9.54	9.50	9.64	9.51	9.44	9.40	9.37	9.24	8.86	9.44	9.36	9.26
NGC 7793	9.67	9.38	9.69	9.63	9.33	9.52	9.56	9.18	9.07	9.60	9.29	9.43
UGC 128	9.85	9.74	9.86	9.81	9.70	9.69	9.73	9.55	9.24	9.78	9.66	9.60
NGC 2403	9.47	9.62	9.86	9.44	9.54	9.52	9.23	9.27	8.85	9.32	9.42	9.33
NGC 925	9.95	9.93	10.01	9.91	9.87	9.75	9.76	9.65	9.19	9.83	9.79	9.61
NGC 2903	10.35	10.48	10.19	10.32	10.42	9.97	10.20	10.23	9.46	10.25	10.35	9.85
NGC 3198	10.03	10.16	10.28	9.99	10.08	9.97	9.81	9.83	9.34	9.89	9.974	9.80
NGC 3621	9.88	9.88	10.31	9.84	9.819	10.06	9.71	9.62	9.53	9.77	9.743	9.93
NGC 3521	10.45	10.53	10.79	10.42	10.49	10.65	10.37	10.36	10.24	10.40	10.46	10.58
NGC 3031	10.81	10.86	10.85	10.77	10.85	10.80	10.80	10.79	10.48	10.80	10.87	10.78
NGC 5055	10.63	10.73	10.95	10.59	10.69	10.78	10.52	10.55	10.35	10.56	10.65	10.70
NGC 2998	10.84	...	10.99	10.80	...	10.70	10.63	...	10.09	10.71	...	10.53
NGC 2841	10.90	11.01	11.07	10.86	10.98	10.98	10.84	10.89	10.61	10.86	10.98	10.93
NGC 6674	10.92	...	11.17	10.88	...	10.96	10.77	...	10.46	10.83	...	10.84
NGC 7331	10.78	10.95	11.23	10.74	10.90	11.06	10.67	10.75	10.61	10.71	10.86	10.97
NGC 801	11.02	...	11.24	10.98	...	11.05	10.90	...	10.59	10.94	...	10.95
NGC 5533	11.17	...	11.31	11.14	...	11.24	11.14	...	10.88	11.15	...	11.20
UGC 2885	11.24	...	11.46	11.20	...	11.18	11.04	...	10.60	11.12	...	11.02

Notes. Masses are base ten logarithms in $M_\odot$. For each population model, the mass estimate from the V-band luminosity is given first, then that from the I band, then the [3.6] luminosity. The models used are those of Bell et al. (2003, B03), Portinari et al. (2004, P04), Zibetti et al. (2009, Z09), and Into & Portinari (2013, IP13).

In the mean time, considerable caution is warranted in assigning stellar masses based on SED fits (Conroy & Gunn 2010). The results will depend not only on the model adopted, but also on the range of wavelengths fit. The offset between optical and NIR luminosity discussed here will result in a systematic skew towards lower stellar masses as more NIR data are incorporated into SED fits. Other fit parameters, like the star formation rate, will also be affected.

5. SELF-CONSISTENT CMLR

Here we consider what is necessary to make empirically self-consistent CMLR. We note first that all models provide a reasonably consistent picture in the optical. This is not surprising given the optical heritage of the subject, and that the difficulty in modeling the latest stages of stellar evolution mostly impacts the NIR. We therefore adopt the V band as a reference point that is well grounded in Galactic star counts (Flynn et al. 2006).

5.1. Self-Consistent Stellar Masses

The relation between the mass computed in one band and that in another appears well defined, if not the desired 1:1 ratio (Figure 2). We begin by fitting linear relations between the stellar mass in band $j = I$ and [3.6] and that in V of the form

$$\log(M_*^j/M_0) = B_j \log(M_*^V/M_0). \quad (3)$$

Here B_j is the slope of the fitted line, and M_0 the mass where the V band and band j intersect. The fitted lines are shown in Figure 2 and reported in Table 4.

These lines provide a mapping between the mass in the reference V band and that in the other filters. They represent what is needed to obtain self-consistency within the context of each model. They do not tell us what is right in an absolute sense, but they do tell us what would, on average, return the same stellar mass from luminosities measured in each band.

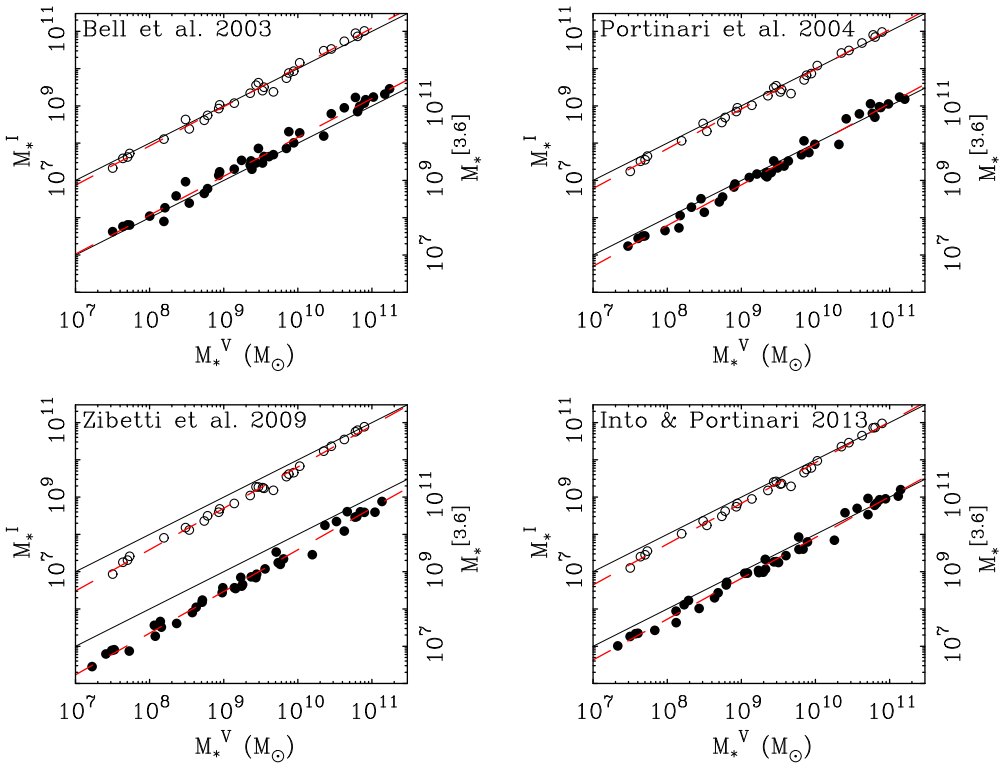

Figure 2. Stellar masses (Table 3) estimated by population synthesis models (Bell et al. 2003; Portinari et al. 2004; Zibetti et al. 2009; Into & Portinari 2013, Table 2). For each model, the mass estimated from the either the *I*-band (open circles) or [3.6] luminosity (filled circles) of each galaxy is plotted against that estimated from the *V*-band luminosity. The two cases are offset for clarity. If the models were perfect the data would follow the solid lines of unity, modulo the expected intrinsic scatter in the relation between the mass-to-light ratio and color. Dashed lines show fits to the data (Table 4) quantifying the deviation from this ideal. These all have slopes greater than unity, indicating that the sensitivity of the mass-to-light ratio to color in *I* and [3.6] is overstated relative to that in *V*. The models also tend to over-predict the [3.6] luminosity relative to the optical luminosity, with the exception of the model of Bell et al. (2003), which underestimates it.

(A color version of this figure is available in the online journal.)

Table 4
Self-Consistent Stellar Masses

Model	$\log(M_0^I)$	B_I	$\log(M_0^{[3.6]})$	$B_{[3.6]}$
Bell et al. (2003)	9.393	1.054	6.431	1.043
Portinari et al. (2004)	10.262	1.067	10.315	1.091
Zibetti et al. (2009)	11.719	1.109	13.531	1.118
Into & Portinari (2013)	10.779	1.094	10.913	1.095

Notes. Fits to the data in Figure 2 that reconcile stellar masses from the *I* band and [3.6] with those from the *V* band such that $\log(M_*^j/M_0) = B_j \log(M_*^V/M_0)$, where B_j is the slope of the fitted line, and M_0 the mass where the *V* band and band $j = I$ or [3.6] intersect.

Note that in all cases the slope $B_j > 1$. Higher mass galaxies are generally redder, so the slope B presumably reflects a misestimate of the color slopes b_j tabulated in Table 2. These are generally too large, in the sense that the mass-to-light ratios in the redder bands of real galaxies do not vary as much with color as expected.

5.2. Primary Color Dependence

We use the lines fit in Figure 2 and Table 4 to estimate a revised mass-to-light ratio for each galaxy in both *I* and [3.6]. In effect, we assume that the mass indicated by the *V* band is correct, and renormalize the other bands accordingly. We then plot these against color to search for a revised CMLR that is self-consistent within the context of each model. The revised mass-to-light ratios are plotted against $B - V$ in Figure 3, $V - I$ in Figure 4, and $J - K_s$ in Figure 5.

There exist reasonably well defined CMLRs in Figure 3: Υ_* does correlate with $B - V$, if not quite with the expected slope. The same cannot be said of the redder colors. There is little if any perceptible slope of Υ_* with either $V - I$ (Figure 4) or $J - K_s$ (Figure 5), and a great deal of scatter in most cases. While these colors may be useful as metallicity indicators (e.g., Bell & de Jong 2000), they appear to have little power to predict Υ_*. This is consistent with the expectations of our own models (Section 3; Schombert & Rakos 2009; Schombert & McGaugh 2014a), and with our unsatisfactory experience in attempting to use these colors to build the equivalent of Table 3 (Section 4).

We fit lines to the data in Figure 3 and provide the resulting self-consistent CMLR[7] in Table 5. These are shown in Figure 6. The agreement between models for the CMLR in the *I* band is greatly improved. That at [3.6] is also better, though considerable differences remain (compare Figure 6 to Figure 1).

Among the four population synthesis models considered here, those of Bell et al. (2003) and Portinari et al. (2004) require the smallest corrections. The corrections to the models of Zibetti et al. (2009) and Into & Portinari (2013) are rather larger. As anticipated, the revised slopes β_j become shallower than the corresponding b_j for all models in Table 2. The corrections to the older models are plausibly at the level one might expect. For the newer models, both the slope and intercept of the CMLR change substantially. The revised CMLR in Figure 3 also has more scatter for the newer models than for the older models.

[7] The $B - V$ color maps closely to $g - r$ (Jester et al. 2005), so it should be straightforward to translate these CMLR into SDSS bands if desired.

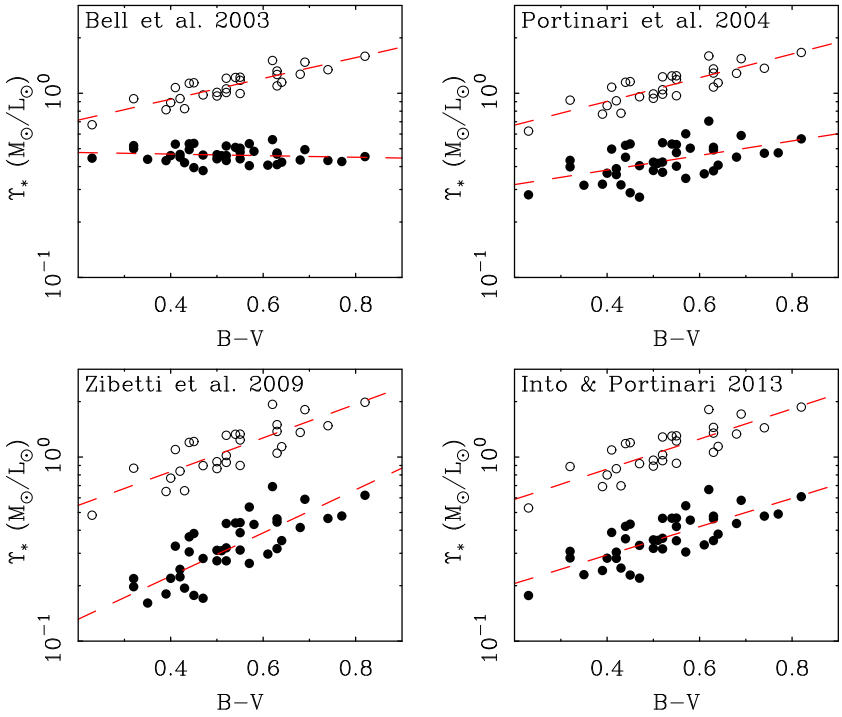

Figure 3. Stellar mass-to-light ratios in the *I* band (open circles) and [3.6] (filled circles) as a function of $B-V$ color. The models of Bell et al. (2003), Portinari et al. (2004), Zibetti et al. (2009), and Into & Portinari (2013) have been revised according to the fits in Table 4. Fits to the data (dashed lines) are given in Table 5. There is scatter in the data because the $V-I$ and $V-[3.6]$ colors of a galaxy vary at a given $B-V$. Note that the bluest galaxies falls off the graph with $\Upsilon_*^{[3.6]} < 0.1\ M_\odot/L_\odot$ in the lower left plot.

(A color version of this figure is available in the online journal.)

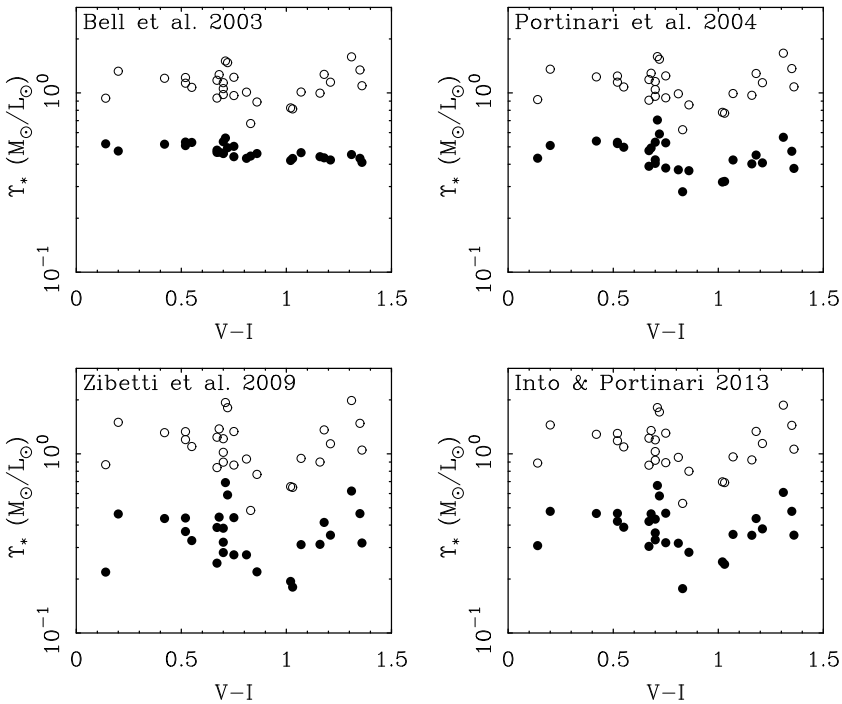

Figure 4. Stellar mass-to-light ratios in the *I* band (open circles) and [3.6] (filled circles) as a function of $V-I$ color. The models of Bell et al. (2003), Portinari et al. (2004), Zibetti et al. (2009), and Into & Portinari (2013) have been revised according to the fits in Table 4. Contrary to the case of $B-V$ (Figure 3), there is little correlation: $V-I$ is not a good primary indicator of Υ_*, though it does have some value as a secondary indicator when combined with $B-V$ (Figure 8).

It appears that the more recent models do not provide an improved description of real galaxies.

The most obvious culprit for the degraded performance of the newer models is an overestimate of the contribution to the NIR light by TP-AGB stars. These stars hardly affect the *V* band while the *I* band and [3.6] are both strongly affected. It appears that well-intentioned attempts to incorporate the latest evolutionary tracks for TP-AGB stars have caused the more recent models

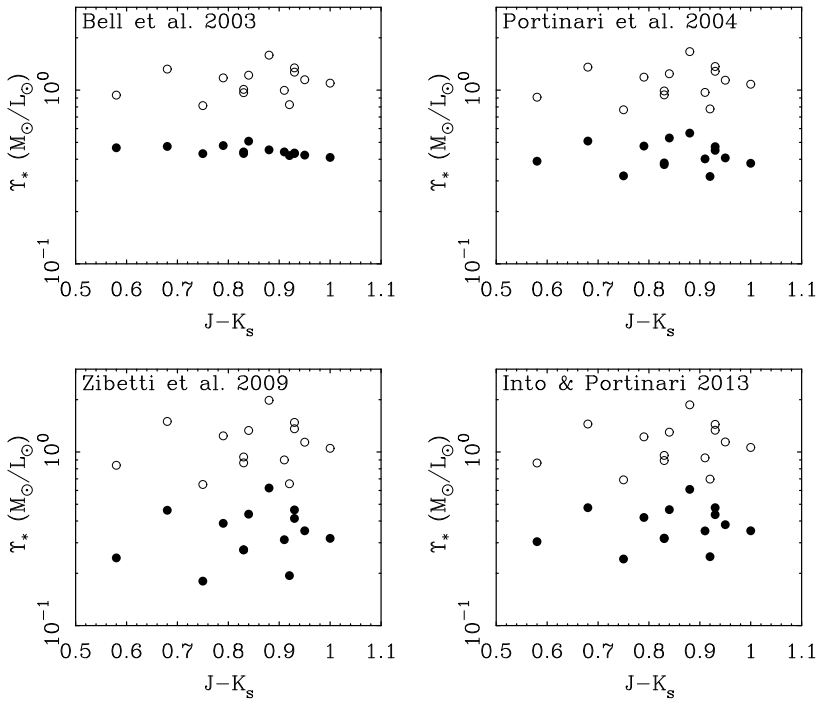

Figure 5. Stellar mass-to-light ratios in the I band (open circles) and [3.6] (filled circles) as a function of $J - K_s$ color. The models of Bell et al. (2003), Portinari et al. (2004), Zibetti et al. (2009), and Into & Portinari (2013) have been revised according to the fits in Table 4. Contrary to the case of $B - V$ (Figure 3), there is little correlation: $J - K_s$ does not provide a good indicator of Υ_*.

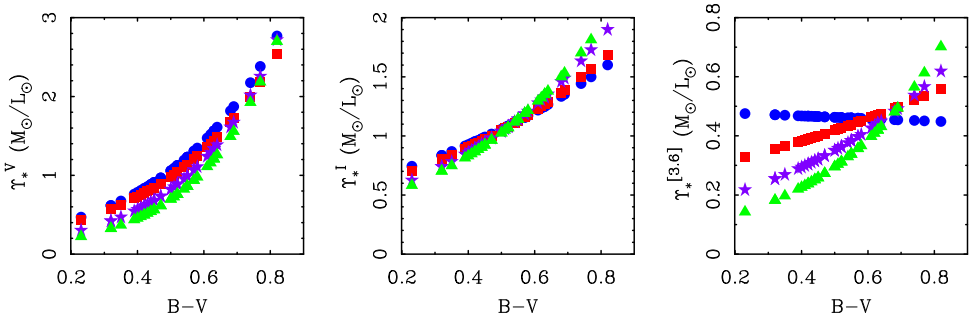

Figure 6. Relation between $B - V$ color and the stellar mass-to-light ratio in the V band (left), I band (center) and the *Spitzer* [3.6] band (right) after correction of each stellar population model (Table 5) to obtain self-consistency. Symbols as in Figure 1. The V-band panel is identical to that in Figure 1 as the models have been self-normalized to that band. Agreement between the models is improved in the other bands, though perceptible differences persist.

(A color version of this figure is available in the online journal.)

Table 5
Self-Consistent Population Synthesis CMLR

Model	a_V	b_V	α_I	β_I	$\alpha_{[3.6]}$	$\beta_{[3.6]}$	$\Upsilon^V_{0.6}$	$\Upsilon^I_{0.6}$	$\Upsilon^K_{0.6}$	$\Upsilon^{[3.6]}_{0.6}$
Bell et al. (2003)	−0.628	1.305	−0.259	0.565	−0.313	−0.043	1.43	1.20	0.60	0.46
Portinari et al. (2004)	−0.654	1.290	−0.302	0.644	−0.575	0.394	1.32	1.22	0.60	0.46
Zibetti et al. (2009)	−1.075	1.837	−0.446	0.915	−1.115	1.172	1.07	1.27	0.50	0.39
Into & Portinari (2013)	−0.900	1.627	−0.394	0.820	−0.841	0.771	1.19	1.25	0.54	0.42

Notes. Stellar mass-to-light ratios in the V, I, and K bands given by the formula $\log \Upsilon^j_* = \alpha_j + \beta_j(B - V)$. For each model, the V band is identical to that in Table 2, but the I and [3.6] bands have been revised to attain self-consistency with the V band (see text). The resulting lines are the fits shown in Figure 3. For reference, the mass-to-light ratio at $B - V = 0.6$ is also given. For K_s, we assume $K_s - [3.6] = 0.31$ (the mean observed color) so that $\Upsilon^K_* = 1.29\Upsilon^{[3.6]}_*$.

to deviate further from reality than the preceding generation of models.

Indeed, the results here can be used to inform future modeling efforts. The self-consistent CMLR provide a benchmark for comparison to models, which should obtain the same spectral shape for a given stellar mass. In addition to defining the general trend of Υ_* with color, the self-consistent CMLR might also help identify specific populations of stars that may affect particular parts of the spectrum, TP-AGB stars being the obvious example here.

5.3. Secondary Color Dependence

The $B - V$ color provides the best primary indicator of Υ_* among the available colors (Figures 3–5). While we find $V - I$ and $J - K_s$ to be unsatisfactory in this regard, that does not mean they are completely devoid of information. Here we search for

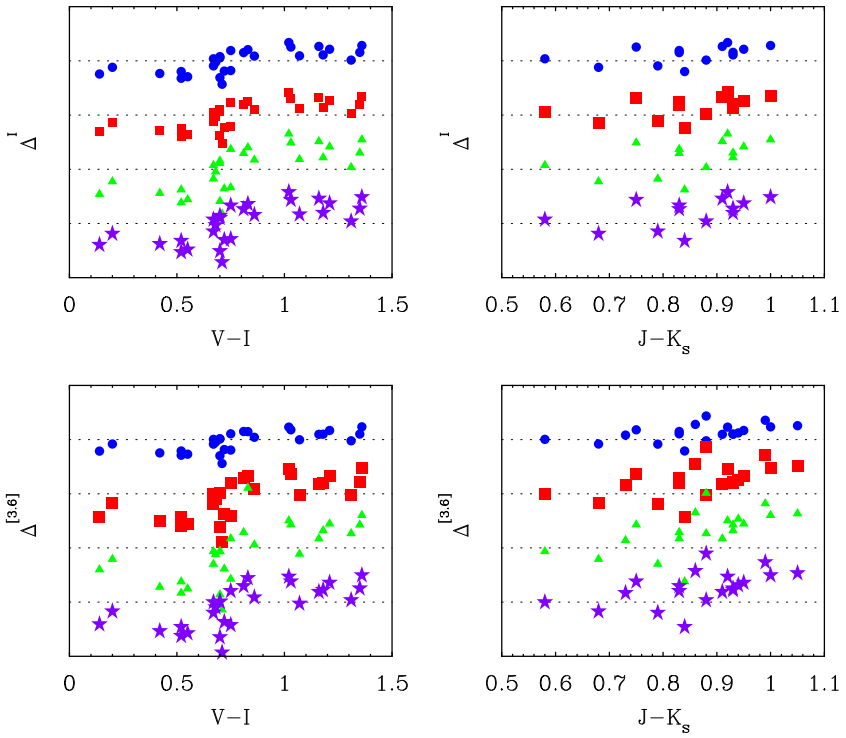

Figure 7. Offset in mass-to-light ratios in the *I*-band (top row) and [3.6] (bottom row) as a function of a second color: $V-I$ (left column) and $J-K$ (right column). Δ is the logarithmic offset between the mass-to-light ratio that gives self-consistent stellar masses (Table 4) and that approximated from the mean trend with $B-V$ color (Table 5). The offsets for each population model have been shifted for clarity (symbols are per Figure 1). Zero offset is shown by the dotted lines, which are offset from each other by 0.2 dex. Deviations of the data from these lines show when extra information about the mass-to-light ratio is provided by the secondary color above and beyond that predicted by $B-V$ (Table 6). The trend is as expected: redder colors indicate higher mass-to-light ratios. The effect of $V-I$ is essentially binary: there is an approximately constant shift in Υ_* above or below $V-I \approx 0.7$. There is rather less information in $J-K_s$, though very red galaxies do tend to have higher Υ_*. The modest amplitude of these shifts imply that a single optical color contains most but not all of the information that can be used to constrain Υ_*.

(A color version of this figure is available in the online journal.)

Table 6
Second Color Correction Terms

Model	$V-I<0.65$		$V-I>0.75$		$J-K>0.90$	
	Δ^I	$\Delta^{[3.6]}$	Δ^I	$\Delta^{[3.6]}$	Δ^I	$\Delta^{[3.6]}$
Bell et al. (2003)	−0.047	−0.044	0.036	0.024	0.046	0.037
Portinari et al. (2004)	−0.057	−0.089	0.045	0.048	0.057	0.075
Zibetti et al. (2009)	−0.089	−0.118	0.070	0.075	0.089	0.099
Into & Portinari (2013)	−0.077	−0.093	0.062	0.053	0.078	0.079

Notes. Corrections to the stellar mass-to-light ratio from a second color term, either $V-I$ or $J-K$ (not both). The tabulated Δ for each band and color range can be added to the formula from Table 5 to improve the estimate of stellar mass-to-light ratio: $\log \Upsilon_*^j = \alpha_j + \beta_j(B-V) + \Delta^j$ when the second color is available. $\Delta = 0$ for color ranges not listed: $0.65 \leqslant V-I \leqslant 0.75$ and $J-K \leqslant 0.9$.

improvements to the primary CMLR by including these colors as a secondary term.

The CMLR in Table 5 is based on a fit against color of the stellar mass that is estimated through the procedure described in Section 5.1. As such, they are not guaranteed to perfectly reproduce the input. Indeed, there is a fair amount of scatter in Figure 3, though some scatter is expected just from variations in the star formation history.

To check if some further improvement can be obtained, we define an offset Δ^j for $j = I, [3.6]$. This is simply the difference between the mass-to-light ratio given by the relation in Table 4 and that in Table 5. This is the residual between the data and the line in Figure 3.

We plot the residual offset Δ^j against $V-I$ and $J-K_s$ in Figure 7. There is a clear effect with $V-I$: blue galaxies are offset to lower Υ_*, and red ones to higher Υ_* than nominally anticipated by the CMLR of Table 5. There is little effect in $J-K_s$, though the reddest galaxies do show some offset. In both cases, the effect goes in the expected[8] sense: galaxies that are bluer in $V-I$ at a given $B-V$ have a lower Υ_*, and those that are redder in either $V-I$ or $J-K_s$ at fixed $B-V$ have higher Υ_*.

We give a correction term as a function of color in Table 6. We treat this term as a simple step function offset. This describes the $V-I$ data quite well outside a narrow transition region. The $J-K_s$ data give the visual impression of a linear rise in

[8] There is a hint in Figure 4 that in the model of Bell et al. (2003) $\Upsilon_*^{[3.6]}$ declines a small amount as $V-I$ becomes redder. This is not apparent in the other models, and may be an artifact of the slight overestimate of $\Upsilon_*^{[3.6]}$ in this case (Figure 2). This trend, if real, only happens when $V-I$ is used as a primary indicator. When used as a secondary indicator, galaxies that are redder at a given $B-V$ have higher Υ_*, and bluer galaxies have lower Υ_*.

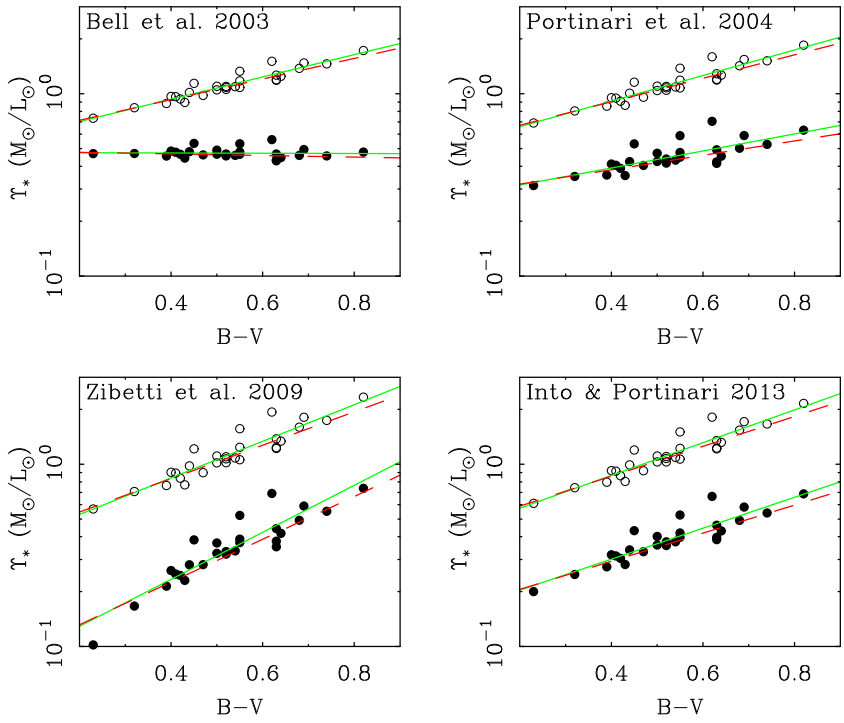

Figure 8. Stellar mass-to-light ratios in the *I* band (open circles) and [3.6] (filled circles) as in Figure 3 corrected with $V - I$ as a second color term as per Table 6. Though the typical correction is less than 0.1 dex, the reduction in scatter is noticeable. The data are re-fit (solid lines) to provide an improved CMLR (Table 7). The previous fits from Figure 3 (dashed lines) are reproduced as here for comparison.

(A color version of this figure is available in the online journal.)

Table 7
Revised CMLR

Model	a_V	b_V	α_I	β_I	$\alpha_{[3.6]}$	$\beta_{[3.6]}$	$\Upsilon^V_{0.6}$	$\Upsilon^I_{0.6}$	$\Upsilon^K_{0.6}$	$\Upsilon^{[3.6]}_{0.6}$
Bell et al. (2003)	−0.628	1.305	−0.275	0.612	−0.322	−0.007	1.43	1.24	0.61	0.47
Portinari et al. (2004)	−0.654	1.290	−0.321	0.701	−0.594	0.467	1.32	1.26	0.63	0.49
Zibetti et al. (2009)	−1.075	1.837	−0.477	1.004	−1.147	1.289	1.07	1.33	0.54	0.42
Into & Portinari (2013)	−0.900	1.627	−0.421	0.898	−0.861	0.849	1.19	1.31	0.58	0.45

Notes. Stellar mass-to-light ratios in the *V*, *I*, and *K* bands given by the formula $\log \Upsilon^j_* = \alpha_j + \beta_j(B - V)$. For each model, the *V* band is identical to that in Table 2, but the *I* and [3.6] bands have been revised to attain self-consistency with the *V* band, and further corrected for $V - I$ as a second color term: the Δ of Table 6 have been incorporated to produce these revised CMLR. The resulting lines are fits to the data in Figure 8, providing our best estimate of the CMLR. For reference, the mass-to-light ratio at $B - V = 0.6$ is also given. For the K_s band, we assume $\Upsilon^K_* = 1.29\Upsilon^{[3.6]}_*$.

Δ redward of a long region of no effect, but the scatter is large enough that there is no perceptible improvement with such a more complicated fit. Indeed, we see little added value in $J - K_s$ as a Υ_* estimator.

There is clear value added in combining $V - I$ with $B - V$ as an indicator of Υ_*. Figure 8 shows the results of correcting the formulae in Table 5 with Δ from Table 6. The best fit line is only slightly changed; these slight revisions to the CMLR are given in Table 7. Perhaps the most remarkable change is that the scatter is greatly reduced, perhaps as much as one could reasonably hope. Consequently, $B - V$ and $V - I$ appear to contain nearly all the information about Υ_* that the SED has to offer, at least for $\lambda > 4000$ Å (UV colors appears promising for elliptical galaxies: Zaritsky et al. 2014).

6. DISCUSSION

6.1. Estimating Stellar Mass-to-Light Ratios

Examining Figure 8 and Table 7, it becomes apparent that stellar masses consistent with the *V*-band estimates are only obtained if the mass-to-light ratios in the redder bands are relatively heavy. The absolute range in both Υ^I_* and $\Upsilon^{[3.6]}_*$ is now much narrower than originally predicted. Comparing their value at a fiducial color of $B - V = 0.6$ in Tables 2 and 7, we find the range of the *I*-band mass-to-light ratio has changed from $0.76 < \Upsilon^I_* < 1.25\ M_\odot/L_\odot$ to $1.24 < \Upsilon^I_* < 1.33\ M_\odot/L_\odot$, while that at [3.6] has narrowed from $0.14 < \Upsilon^{[3.6]}_* < 0.62\ M_\odot/L_\odot$ to $0.42 < \Upsilon^{[3.6]}_* < 0.49\ M_\odot/L_\odot$. Factors of two (or more) variation have been reduced to <20%. This would appear to validate the long standing intuition that redder bands would provide the more direct measure of stellar mass.

Looking at the individual models, the revised CMLR based on the model of Bell et al. (2003) has the least scatter. The model of Portinari et al. (2004) is very nearly as good. The scatter becomes progressively worse in the models of Into & Portinari (2013) and Zibetti et al. (2009). This is not surprising since the revised CMLR of the latter have had gross corrections to both their intercept and slope. These models did not have their NIR luminosities in the right ballpark to begin with.

Comparing the models of Bell et al. (2003) and Portinari et al. (2004), the revised CMLR in the I band are practically indistinguishable. At [3.6], the two differ slightly in that the revised CMLR of the Bell et al. (2003) model has effectively zero color dependence, while that of Portinari et al. (2004) does show a shallow slope. The latter is nonzero at $\sim 2.5\sigma$ significance, so there is formally some slight tension between the models. This seems a reasonable amount of agreement given the various uncertainties. For example, we tried varying the prescription for internal extinction from zero to the RC3 (de Vaucouleurs et al. 1991) prescription, with results intermediate between those in Tables 5 and 7. These bracketing cases are not much different, and such differences are much smaller than the uncertainty in the IMF.

As a practical matter, the mass-to-light ratio in the NIR is effectively constant. The revised Bell et al. (2003) model has $\langle \Upsilon_*^{[3.6]} \rangle = 0.47\ M_\odot/L_\odot$. All galaxies are within 0.1 dex of this mean value. Comparing this with the model of Portinari et al. (2004), 22 of 28 galaxies are within 0.1 dex of $0.47\ M_\odot/L_\odot$, and none deviate by as much as 0.2 dex. Even the model of Zibetti et al. (2009), with its different IMF, larger scatter, and much stronger color dependence is largely consistent with this mean value but for galaxies with extreme colors.

It therefore seems advisable to adopt $\Upsilon_*^{[3.6]} = 0.47\ M_\odot/L_\odot$ as a characteristic value, with corresponding value $\Upsilon_*^K = 0.6\ M_\odot/L_\odot$. There is no clear need to correct these mean values with color terms. Indeed, the range of variation implied by the slope of the Portinari et al. (2004) model is comparable to the scatter. It therefore appears unwise to attempt any color correction in these bands, as one is as likely to add noise as to improve the situation. A corollary is that a NIR image is already as good a map of the stellar mass as it is possible to obtain.[9]

In principle, one would expect that by using all of the spectral information by fitting the complete SED, one would obtain the best stellar mass estimate. In practice, this does not appear to be true: population synthesis models are not yet up to this task. Mismatches between models and reality will inevitably introduce systematic errors into any such procedure. In practice, one is better off simply assuming a constant Υ_* in the NIR.

In contrast to the NIR, a clear color dependence persists in the I band. Unlike [3.6], the I-band luminosity does not provide a direct measure of stellar mass. Nevertheless, Figure 8 gives reason to hope that a simple color correction, as provided in Table 7, or the combination of Tables 5 and 6, can be utilized to provide a reasonable estimate of stellar mass. This is not as good as measuring the NIR luminosity directly, but is often more readily obtained.

Note that a $B - V$ color is needed to estimate Υ_*^I; $V - I$ by itself is no help. If only B and V are available without the I band, then one is back to relying on the population synthesis models, which appear to be fairly robust in the optical. If only a single bandpass is available, to a crude first approximation, $\Upsilon_* \approx 1.2\ M_\odot/L_\odot$ in each of B, V, and I.

The absolute values of the mass-to-light ratios given here explicitly assume that the modeling of the optical portion of the spectrum is essentially correct. Really the data only constrain the ratio of optical-to-NIR luminosity to be higher than most models indicate so that $\Upsilon_*^V/\Upsilon_*^{[3.6]} \approx 2.5$–3. One is free to adjust the normalization of both optical and NIR mass-to-light ratios so long as this ratio is preserved, for example by altering the IMF.

[9] We are aware of a variety of attempts to build stellar mass maps by making color corrections to an image. Indeed, we have exerted no small effort along these lines ourselves. As well motivated as these attempts are, they do not appear capable of providing an improvement over the direct NIR image given the present state of model development.

6.2. Comparison with Independent Constraints

There are independent constraints that we can check Υ_* against. One obvious example is star counts in the Milky Way. For the solar cylinder, Flynn et al. (2006) measure $B - V = 0.58$ and $V - I = 0.90$ (their Table 5). They estimate the stellar mass-to-light ratios of the Milky Way to be $\Upsilon_*^V = 1.5$ and $\Upsilon_*^I = 1.2\ M_\odot/L_\odot$ (both ± 0.2). This compares favorably with the $B - V = 0.6$ values in Table 7, where $\Upsilon_*^V = 1.43$ and $\Upsilon_*^I = 1.24\ M_\odot/L_\odot$ for the revised Bell et al. (2003) CMLR. Staying with this model to be specific, we can apply the formulae we have derived to the observed colors. Applying the formula from Table 5, which depends only on $B - V$, we obtain $\Upsilon_*^I = 1.17\ M_\odot/L_\odot$. Correcting this with $V - I$ as a second term as per Table 6, we obtain $\Upsilon_*^I = 1.27\ M_\odot/L_\odot$. The formula in Table 7 (which depends only on $B - V$) gives $\Upsilon_*^I = 1.20\ M_\odot/L_\odot$. This gives an idea of the consistency and precision that can be obtained.

Eskew et al. (2012) calibrate the conversion between NIR flux and stellar mass in the LMC. They obtain $\Upsilon_*^{[3.6]} = 0.5\ M_\odot/L_\odot$, in excellent agreement with our results. Eskew et al. (2012) further discuss a [3.6]–[4.5] color correction to this basic result. Given the lack of sensitivity of Υ_* to $J - K_s$ that we find, and the small scatter (0.11 mag.) that we measure in $K_s - [3.6]$, we find it unlikely that the [3.6]–[4.5] color provides much information to improve estimations of Υ_* in the NIR. Irrespective of this detail, our basic results are in very good agreement.

Star count constraints, though direct, are still subject to uncertainty in the IMF. We can also compare our results to dynamical constraints. For example, Bovy & Rix (2013) have recently measured the vertical force in the Milky Way disk over a substantial range of radii outside the solar circle. Their results are consistent with the Milky Way model constructed by McGaugh (2008) based on the work of Flynn et al. (2006). Consequently, the implied mass-to-light ratios are also consistent.

The vertical force in external disk galaxies also provides a constraint. Our results are simultaneously consistent and in conflict with those of the disk mass survey (Bershady et al. 2010). Martinsson et al. (2013) find that essentially all disk galaxies have indistinguishable mass-to-light ratios in the K band, just as we do. However, their normalization is different: Martinsson et al. (2013) find $\langle \Upsilon_*^K \rangle = 0.31 \pm 0.07$. This is basically a factor of two lower than the corresponding values in Table 7.

The lower mass scale favored by the disk mass survey (e.g., Bershady et al. 2011) could readily be obtained through a simple renormalization. As mentioned previously, all that we require here is the correct ratio between optical and NIR luminosities. Whether this can be reconciled with measurements on the IMF and other known dynamical constraints (e.g., Sellwood 1999) is beyond the scope of this work. We see no clear cut reason to prefer one mass scale over another, so a systematic uncertainty of a factor of ~ 2 persists in the absolute stellar mass scale.

The Baryonic Tully–Fisher relation (McGaugh et al. 2000) provides another constraint. Using the calibration based on gas rich galaxies of McGaugh (2012), we have checked the implied NIR mass-to-light ratios for those galaxies discussed here for which adequate kinematic data exist. This is an independent check, as the baryonic mass is estimated from

the observed rotation velocity as calibrated by galaxies where the stars do not contribute substantial systematic uncertainty to the baryonic mass budget (McGaugh 2011). The resulting stellar mass estimate follows from the kinematically estimated baryonic mass less the observed gas mass; it is not informed by the purely photometric results here. We find typical NIR mass-to-light ratios in the range $\Upsilon_*^{[3.6]} = 0.4$–$0.5\ M_\odot/L_\odot$, consistent with our results in Table 7 (and by implication, heavier than those of the disk mass survey, but consistent with the Milky Way and LMC). We will explore this further in a companion paper.

7. CONCLUSIONS

We have used *Spitzer* data for disk galaxies spanning 10 magnitudes in [3.6] absolute magnitude to test the self-consistency of stellar population synthesis models from the optical to NIR bands. Our main conclusions can be summarized as follows.

1. Many commonly utilized stellar population models are not self-consistent in the sense that application of the same model to the same galaxy results in different stellar masses depending on whether an optical or NIR luminosity is used.
2. Ab initio models tend to overestimate the NIR luminosity relative to the optical luminosity for a given mass of stars.
3. Models adopting recent prescriptions for TP-AGB stars severely overstate the NIR luminosity.
4. Self-consistency between optical and NIR observations can be achieved if NIR mass-to-light ratios are approximately constant.
5. The typical value for self-consistency is $0.47\ M_\odot/L_\odot$ at $3.6\,\mu$m (equivalent to $0.6\ M_\odot/L_\odot$ in the K_s band).
6. The mass-to-light ratio in optical bands does depend on $B-V$ color (see Table 7). Redder colors like $J-K_s$ carry little additional information.

Workers wishing to estimate the stellar masses of galaxies would do well to adopt a constant NIR mass-to-light ratio as calibrated here. If NIR bands such as K_s or [3.6] are not available, the mass-to-light ratio in bluer bands like I do correlate with a $B-V$ color. This color contains most of the information about Υ_*. A slight improvement can be gained by using $V-I$ as a secondary indicator. Redder colors like this and $J-K_s$ have themselves no power as primary predictors of Υ_*.

Once a NIR luminosity is measured, there appears to be little added value in fitting the complete SED so far as constraining the stellar mass goes. Indeed, such fits can only be as good as the population model the data are fit to. Given the systematic offsets in the models found here, such SED fits are bound to suffer from systematic errors that will depend on the specific model employed and also on the range of wavelengths fit. On the other hand, the results found here can be used to inform improvements in the models.

We thank Laura Portinari and the referee for numerous helpful suggestions. This work is based in part on observations made with the *Spitzer Space Telescope*, which is operated by the Jet Propulsion Laboratory, California Institute of Technology under a contract with NASA. Support for this work was provided by NASA through an award issued by JPL/Caltech. Other aspects of this work were supported in part by NASA ADAP grant NNX11AF89G and NSF grant AST 0908370. This research has made use of the NASA/IPAC Extragalactic Database (NED) which is operated by the Jet Propulsion Laboratory, California Institute of Technology, under contract with the National Aeronautics and Space Administration.

REFERENCES

Bell, E. F., & de Jong, R. S. 2000, MNRAS, 312, 497
Bell, E. F., & de Jong, R. S. 2001, ApJ, 550, 212
Bell, E. F., McIntosh, D. H., Katz, N., & Weinberg, M. D. 2003, ApJS, 149, 289
Bershady, M. A., Martinsson, T. P. K., Verheijen, M. A. W., et al. 2011, ApJL, 739, L47
Bershady, M. A., Verheijen, M. A. W., Swaters, R. A., et al. 2010, ApJ, 716, 198
Bovy, J., & Rix, H.-W. 2013, ApJ, 779, 115
Bruzual, G., & Charlot, S. 2003, MNRAS, 344, 1000
Chabrier, G. 2003, ApJL, 586, L133
Conroy, C., & Gunn, J. E. 2010, ApJ, 712, 833
Dale, D. A., Bendo, G. J., Engelbracht, C. W., et al. 2005, ApJ, 633, 857
Dale, D. A., Gil de Paz, A., Gordon, K. D., et al. 2007, ApJ, 655, 863
de Blok, W. J. G., van der Hulst, J. M., & Bothun, G. D. 1995, MNRAS, 274, 235
de Blok, W. J. G., Walter, F., Brinks, E., et al. 2008, AJ, 136, 2648
de Vaucouleurs, G., de Vaucouleurs, A., Corwin, H. G. Jr., et al. 1991, Third Reference Catalogue of Bright Galaxies (New York: Springer)
Eskew, M., Zaritsky, D., & Meidt, S. 2012, AJ, 143, 139
Fisher, D. B., & Drory, N. 2008, AJ, 136, 773
Flynn, C., Holmberg, J., Portinari, L., Fuchs, B., & Jahreiß, H. 2006, MNRAS, 372, 1149
Into, T., & Portinari, L. 2013, MNRAS, 430, 2715
Jarrett, T. H., Chester, T., Cutri, R., et al. 2000, AJ, 119, 2498
Jester, S., Schneider, D. P., Richards, G. T., et al. 2005, AJ, 130, 873
Kennicutt, R. C., Jr., Armus, L., Bendo, G., et al. 2003, PASP, 115, 928
Kim, J. H., Im, M., Lee, H. M., et al. 2012, ApJ, 760, 120
Kriek, M., Labbé, I., Conroy, C., et al. 2010, ApJL, 722, L64
Kroupa, P. 1998, in ASP Conf. Ser. 134, Brown Dwarfs and Extrasolar Planets, ed. R. Rebolo, E. L. Martin, & M. R. Zapatero Osorio (San Francisco, CA: ASP), 483
Le Borgne, D., Rocca-Volmerange, B., Prugniel, P., et al. 2004, A&A, 425, 881
Makarova, L. 1999, A&AS, 139, 491
Maraston, C. 2005, MNRAS, 362, 799
Marigo, P., Girardi, L., Bressan, A., et al. 2008, A&A, 482, 883
Martinsson, T. P. K., Verheijen, M. A. W., Westfall, K. B., et al. 2013, A&A, 557, A131
McGaugh, S. S. 2008, ApJ, 683, 137
McGaugh, S. S. 2011, PhRvL, 106, 121303
McGaugh, S. S. 2012, AJ, 143, 40
McGaugh, S. S., & Bothun, G. D. 1994, AJ, 107, 530
McGaugh, S. S., Schombert, J. M., Bothun, G. D., & de Blok, W. J. G. 2000, ApJL, 533, L99
Meidt, S. E., Schinnerer, E., Knapen, J. H., et al. 2012, ApJ, 744, 17
Melbourne, J., Williams, B. F., Dalcanton, J. J., et al. 2012, ApJ, 748, 47
Muñoz-Mateos, J. C., Gil de Paz, A., Zamorano, J., et al. 2009, ApJ, 703, 1569
Oh, S., de Blok, W. J. G., Walter, F., Brinks, E., & Kennicutt, R. C. 2008, AJ, 136, 2761
Portinari, L., Sommer-Larsen, J., & Tantalo, R. 2004, MNRAS, 347, 691
Schlafly, E. F., & Finkbeiner, D. P. 2011, ApJ, 737, 103
Schombert, J. M. 2011, ascl soft, 7011
Schombert, J. M., Maciel, T., & McGaugh, S. S. 2011, AdAst, 2011, 143698
Schombert, J. M., & McGaugh, S. S. 2014a, PASA, in press (arXiv:1407.6778)
Schombert, J. M., & McGaugh, S. S. 2014b, PASA, 31, 11
Schombert, J. M., & Rakos, K. 2009, AJ, 137, 528
Sellwood, J. A. 1999, in ASP Conf. Ser. 182, Galaxy Dynamics: A Rutgers Symposium, ed. D. R. Merritt, M. Valluri, & J. A. Sellwood (San Francisco, CA: ASP), 351
Trachternach, C., de Blok, W. J. G., McGaugh, S. S., van der Hulst, J. M., & Dettmar, R. 2009, A&A, 505, 577
Tully, R. B., Rizzi, L., Shaya, E. J., et al. 2009, AJ, 138, 323
Verheijen, M. A. W. 2001, ApJ, 563, 694
Walter, F., Brinks, E., de Blok, W. J. G., et al. 2008, AJ, 136, 2563
Zaritsky, D., Gil de Paz, A., & Bouquin, A. Y. K. 2014, ApJL, 780, L1
Zibetti, S., Charlot, S., & Rix, H.-W. 2009, MNRAS, 400, 1181
Zibetti, S., Gallazzi, A., Charlot, S., Pierini, D., & Pasquali, A. 2013, MNRAS, 428, 1479